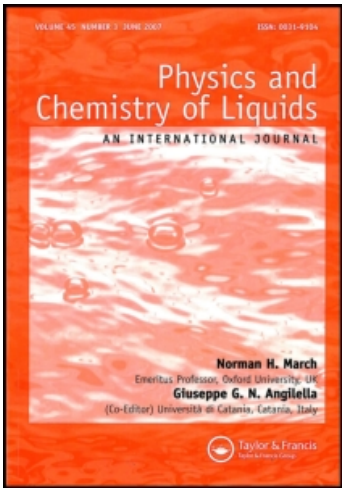

Physics and Chemistry of Liquids
Publication details, including instructions for authors and subscription information:
http://www.informaworld.com/smpp/title~content=t713646857

Comprehensive study of the thermodynamic properties of fullerene C_{60} along the liquid-vapour coexistence

S. M. Osman[a]; M. Bahaa Khedr[b]
[a] Physics Department, College of Science, Sultan Qaboos University, Muscat Sultanate of Oman [b] Physics Department, Faculty of Science, Banha University, Banha, Egypt

To cite this Article Osman, S. M. and Bahaa Khedr, M.(2009) 'Comprehensive study of the thermodynamic properties of fullerene C_{60} along the liquid-vapour coexistence', Physics and Chemistry of Liquids, 47: 5, 564 — 581
To link to this Article: DOI: 10.1080/00319100903096521
URL: http://dx.doi.org/10.1080/00319100903096521

Physics and Chemistry of Liquids
Vol. 47, No. 5, October 2009, 564–581

Taylor & Francis
Taylor & Francis Group

Comprehensive study of the thermodynamic properties of fullerene C_{60} along the liquid–vapour coexistence

S.M. Osman[a]* and M. Bahaa Khedr[b†]

[a]*Physics Department, College of Science, Sultan Qaboos University, P.O. Box 36, P.C. 123, Al_Khod, Muscat Sultanate of Oman;* [b]*Physics Department, Faculty of Science, Banha University, Banha, Egypt*

(*Received 11 April 2009; final version received 7 June 2009*)

We present a theoretical model for calculating the thermodynamic properties of liquid C_{60} by means of an improved equation of state (EOS), in which the particles interact via pairwise interaction composed of hard-core plus suitable linear combinations of three Yukawa functions. The proposed EOS provides simple analytical expressions for Helmholtz free energy and pressure, which are the basic ingredients to compute the liquid–vapour coexistence curve of C_{60} as well as all other thermodynamic properties for the bulk liquid and vapour phases. The comparisons with computer simulation results, based on Girifalco potential, suggest the importance of treating the attractive tail of the potential accurately. It is to be noted that the obtained results of the thermodynamic properties along the binodal curve of C_{60} exhibit interesting features; in particular, the vapour phase shows abnormal behaviour of its isothermal compressibility and configurational heat capacity. The estimated critical parameters $T_c = 2008.8\,\mathrm{K}$, $\rho_c = 0.50\,\mathrm{nm}^{-3}$ and $P_c = 54.8\,\mathrm{bars}$ are in good agreement with NVT-Monte Carlo simulation predictions. The critical parameters of C_{60} are compared with those of liquid metals, non-metals and some hydrocarbons.

Keywords: carbon fullerene C_{60}; thermodynamic properties of C_{60}; equation of state of C_{60}; liquid–vapour coexistence of C_{60}; C_{60} pair potential

1. Introduction

Many carbon fullerenes $C_N \geq 60$ have been synthesised recently, which have shown novel properties and potential applications [1]. The high temperature thermodynamic and structural properties of liquid C_{60} is still of considerable interest from a technological point of view [2]. Several computer simulations [3–6] suggested that the stable liquid phase can only exist in a narrow temperature range ($\approx$100 K).

Theoretical investigations based on density functional theory (DFT) and structure theory have been carried out on C_{60} fluid during the last two decades; for example, two advanced (DFT) approximations: the simplified perturbation weighted density approximation [7] and the generalised modified weighted density approximation [5,8]. Both approaches have predicted the existence of a liquid phase of C_{60} but in a very narrow range of temperature (<20 K), with $T_C = 1960\,\mathrm{K}$. The narrow range of the liquid phase was

*Corresponding author. Email: osm@squ.edu.om
†Permanent address: Faculty of Education, King Khalid University, Bisha, P.O. Box 551, Kingdom of Saudi Arabia.

ISSN 0031–9104 print/ISSN 1029–0451 online

DOI: 10.1080/00319100903096521
http://www.informaworld.com

ascribed [8] to the well-known defect of the modified weighted density approximation, which is due to the shortcoming of the reference system as well as the hard sphere (HS) equation of state (EOS) used. On the other hand, highly accurate structure theories of fluids, such as the modified hypernetted-chain (MHNC) theory [9] can be employed in the determination of the C_{60} phase diagram. The MHNC theory confirmed the existence of a C_{60} liquid phase but with a wider temperature range, 1600–1920 K, for the estimated triple point and critical point of liquid–vapour equilibrium (LVE), respectively (for more details we refer the reader to Bahaa Khedr *et al.* [10]).

Quite recently, theories based on rather sophisticated concepts have been proposed: the hierarchical reference theory (HRT), introduced by Parola and Reatto [11] and the self-consistent Ornstein–Zernike approximation (SCOZA) proposed by Stell and Haye (see, e.g. [12,13]).

The HRT merges ideas of renormalisation group theory with liquid state theory, while the SCOZA starts from the generalised mean spherical approximation enforcing consistency between different thermodynamic routes. The series mean spherical approximation was originally set by Henderson *et al.* [14], reformulated and tested by Duh and Mier-Y-Terán [15]. Most of the work done on C_{60} has led initially to rather controversial results of the position of the critical point on the phase diagram of model fullerene C_{60}. The question whether the liquid phase of fullerenes exists or not is certainly not only of academic but also of technological interest, since fullerenes can be used as lubricants (summarised in Bahaa Khedr *et al.* [10] and Abramo *et al.* [16]).

There are at least five different interfullerene pair potentially proposed for C_{60}. All potential models have the same features of extremely hard core and extremely narrow and deep attractive well. These potentials can be classified into three main categories according to symmetry and rigidity assumptions, as follows. (i) The well-known Girifalco potential, $V_{GR}(r)$ [17],

$$V_{GR}(r) = \alpha\left[\frac{1}{s(s-1)^9} + \frac{1}{s(s+1)^9} - \frac{2}{s^{10}}\right] - \beta\left[\frac{1}{s(s-1)^3} + \frac{1}{s(s+1)^3} - \frac{2}{s^4}\right], \qquad (1)$$

where $s = r/d$, with $d = 7.1$Å, $\alpha = 13.595 \times 10^{-24}$ J and $\beta = 7.494 \times 10^{-21}$ J.

Double Yukawa potential [10,18] and *ab initio* potential of Pacheco and Prates [19] were derived, taking into account the spherical symmetry and rigidity of C_{60} molecules. (ii) The atomistic potential proposed by Abramo *et al.* [20], in which the spatial distribution of carbon atoms within the C_{60} molecule is directly taken into account by fitting a set of adjustable parameters to experimental spectroscopic data. The *ab initio* potential also assumes the symmetry and rigidity of C_{60} molecules. (iii) The size dependent potential was introduced for the first time by Broughton *et al.* [21]: i.e. the non-rigidity assumption, which was introduced via two main parameters, the molecular radius and the softening parameter. These two parameters are considered dynamical variables to fit the empirical breathing frequency mode at low temperatures. It should be mentioned here that all analytical and computer simulations work based on potentials of categories (i) and (ii), confirming the existence of the stable liquid phase, while molecular dynamic simulations [21] that were based on non-rigidity assumption showed meta-stable liquid phase. No doubt the non-rigidity of the molecules had an effect on the characteristics of the liquid phase, but one should be cautious with this model because of its limitations. The recent predictions of accurate computer simulations by Hasegawa and Ohno [22] and by Costa *et al.* [23] testified

that the spherical potential models of categories (i) and (ii) possess a stable liquid phase, which is confined in a rather narrow temperature range.

The second part of this article is devoted to our model potential for C_{60}–C_{60} interaction, for which we suggest a linear combination of three Yukawa functions. In Section 3, we provide explicit expressions for the EOS and some thermodynamic functions of interest. The rest of this work focuses on calculating the LVE curve of C_{60} and discussing the behaviour of important thermodynamic functions along the LVE line, followed with brief conclusions in Section 5.

2. Model potential

The Girifalco potential, Equation (1), is considered the most successful pair interaction for C_{60} molecules as it has been used in almost all reported computer simulations on C_{60} fluid. It has one disadvantage of being analytically impossible to implement within perturbation theory. Therefore, we consider the three Yukawa functions of potential $V_{3YK}(r)$:

$$V_{3YK}(r) = \frac{\varepsilon_0}{x}\left[E_1 e^{-\lambda_1(x-1)} - E_2 e^{-\lambda_2(x-1)} - E_3 e^{-\lambda_3(x-1)}\right], \tag{2}$$

where $x = r/\sigma_0$, with σ_0 being the position of the zero potential and ε_0 the value of the potential minimum position r_m. The two potential functions, $V_{GR}(r)$ and $V_{3YK}(r)$, can be made identical by fitting five points, with reasonable accuracy, inside and outside the attractive bucket, namely,

$$V_{3YK}(r = \sigma_0) = V_{GR}(r = \sigma_0) = 0, \tag{3}$$

$$V_{3YK}(r = r_m) = V_{GR}(r = r_m) = -\varepsilon_0, \tag{4}$$

$$V_{3YK}(r_1) = V_{GR}(r_1) = +\varepsilon_0, \tag{5}$$

$$V_{3YK}(r_2) = V_{GR}(r_2) = -0.5\varepsilon_0, \tag{6}$$

$$V_{3YK}(r_3) = V_{GR}(r_3) = -0.01\varepsilon_0, \tag{7}$$

where $r_1 < \sigma_0 < r_m < r_2 < r_3$,

$$\text{together with the condition } \left.\frac{\partial V_{3YK}(r)}{\partial r}\right|_{r=r_m} = 0. \tag{8}$$

Equation (3) automatically holds for both potentials and leads to the relation $E_3 = E_1 - E_2$. Equations (4) and (8) explicitly determine E_1 and E_2 in terms of λ_1, λ_2 and λ_3. Substituting the obtained expressions of E_1 and E_2 into Equations (5)–(7) facilitates three non-linear equations of λ_1, λ_2 and λ_3, which can be solved numerically by iteration procedure. Table 1 provides the fitting points and the estimated parameters obtained.

Table 1. The 3YK potential parameters for C_{60}.

σ_0Å	r_1/σ_0	r_m/σ_0	r_2/σ_0	r_3/σ_0	
9.5929	0.9880	1.0483	1.1620	1.9199	
ε_0/k_B	E_1	E_2	λ_1	λ_2	λ_3
3218.538	1.7458	1.6077	45.1889	7.4129	2.1648

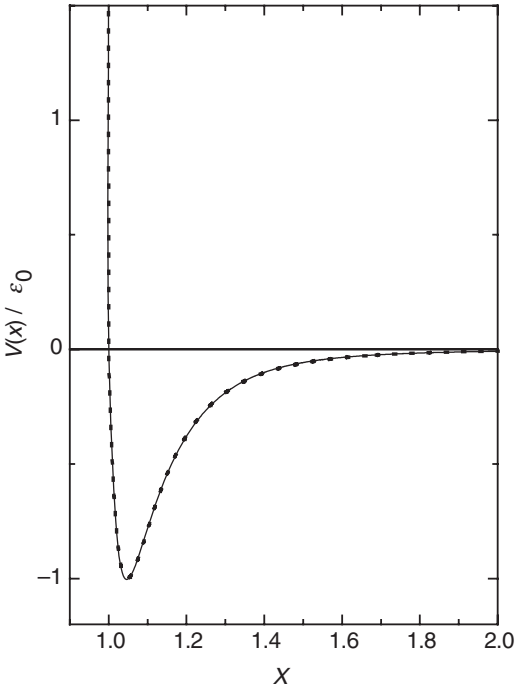

Figure 1. The reduced pair potential of C_{60}, the Girifalco potential $V_{GF}(r)$, [17] (dashed line) and the three Yukawa potential $V_{3YK}(r)$, Equation (2) (solid line), with $x = r/\sigma_\circ$. The C_{60} range and energy parameters are $\sigma_0 = 9.5929$Å and $\varepsilon_0 = 3218.538\,k_B$.

The closest fit of $V_{3YK}(r)$ and $V_{GR}(r)$ is shown in Figure 1. From a statistical mechanics point of view, the two potentials are equivalent if they reproduce the same second virial coefficient $B_2(T)$,

$$B_2(T) = 2\pi \int_0^\infty \left[1 - e^{-\beta V_{3YK}(r)}\right] r^2 \mathrm{d}r. \tag{9}$$

Here $\beta = (k_B T)^{-1} \cdot B_2(T)$ for both $V_{3YK}(r)$ and $V_{GR}(r)$ are presented in Figure 2 by comparing with the molecular dynamic simulation results of Broughton *et al.* [21]. The comparison in Figure 2 shows a close agreement with computer simulation results, which supports the quality of 3YK model potential. Figure 2 also shows that $V_{3YK}(r)$ and $V_{GR}(r)$

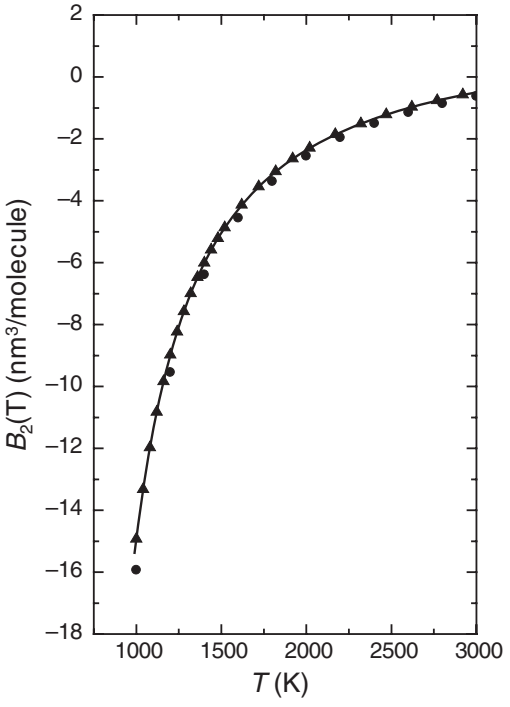

Figure 2. The second virial coefficient of 3YK potential (solid line) calculated via Equation (9) compared with the computer simulation results [21] (solid circles) and with the results of the Girifalco potential [17] (solid triangles).

are predicting precisely the same second virial coefficient over the whole temperature range of liquid and vapour states.

3. Equation of state

We consider a system of N molecules in volume V, with number density $\rho = N/V$ and temperature T. The molecules are interacting via hard-core plus 3YK potential

$$V_{HC3YK}(r) = \begin{cases} \infty & r < \sigma \\ V_{3YK}(r) & r \geq \sigma. \end{cases} \tag{10}$$

We adopt the perturbation scheme [24] to such potential splitting, in which the reference system is chosen to be the HS fluid, and $V_{3YK}(r)$ is considered as perturbation potential. Here, σ is the effective HS diameter. Accordingly, the Helmholtz free energy, F, per particle of the system is the sum of the free energy of the reference system, F_{HS}, plus the contribution from attractive potential tail, F_t. This translates into

$$F(\rho, T) = F_{HS}(y, T) + F_t(y, T), \tag{11}$$

where $y = \frac{\pi}{6}\rho\sigma^3$ is the packing fraction. Similarly, the pressure, P, of the fluid is also a sum of the HS reference system and perturbation contributions, namely

$$P(\rho, T) = P_{HS}(y, T) + P_t(y, T). \tag{12}$$

Regarding the choice of the HS reference system formalism, one can use the popular Carnahan Starling formalism [25], but we choose a suitable combination of usual ideal gas contribution [26] to free energy, $F_{id}(\rho, T)$, plus the scaled particle theory entropy of hard spheres due to Baus and Colot [27], which gives the excess HS Helmholtz free energy, $F_{HS}^{XS}(y, T)$, namely

$$F_{HS}(y, T) = F_{id}(\rho, T) + F_{HS}^{XS}(y, T), \tag{13}$$

$$\frac{\beta F_{id}(\rho, T)}{N} = \ln(\rho) - \frac{3}{2}\ln(T) - 1 - \frac{3}{2}\ln\left[\frac{2\pi m k_B}{h^2}\right], \tag{14}$$

$$\frac{\beta F_{HS}^{XS}(y, T)}{N} = (a + 3b - 1)\ln(1 - y) + \frac{(6 + 2a + 6b)\,y - (3 + 3a + 9b)\,y^2 + 2by^3}{2(1 - y)^2}, \tag{15}$$

and the corresponding HS pressure

$$\frac{\beta P_{HS}(\rho, T)}{\rho} = \frac{1 + y + y^2 - ay^3 - by^4}{(1 - y)^3}, \tag{16}$$

where m and h are the molecular mass and Planck's constant, respectively. Baus and Colot [27] recommended the scaling parameters, $a = b = 3/2$, which provides the most accurate EOS for HS fluids comparable to several other approximations of the HS radial distribution function, $g_{HS}(r, y)$, within the framework of analytical solution of the O–Z integral equation. The perturbation contribution to the Helmholtz free energy is simply

$$\frac{\beta F_t(y, T)}{N} = 12y \int_1^\infty x^2 g_{HS}(x, y)\beta V_{HC3YK}(x)\mathrm{d}x. \tag{17}$$

Here, $x = r/\sigma$. The use of the HC3YK potential, Equation (17), further facilitates analytical expression for F_t by introducing the definition of the Laplace transform of $xg_{HS}(x, y)$, defined as,

$$G(\lambda, y) = \int_0^\infty x g_{HS}(x, y) e^{-\lambda x}\mathrm{d}x. \tag{18}$$

One can, conveniently, introduce the reduced quantities $\sigma^* = \frac{\sigma}{\sigma_0}$, $\lambda^* = \lambda\sigma^*$ and $T^* = (\beta\varepsilon_0)^{-1}$. Then Equation (17) reduces to

$$\frac{\beta F_t(y, T)}{N} = \frac{12y}{T^*}\left[E_1 e^{\lambda_1} G(\lambda_1^*, y) - E_2 e^{\lambda_2} G(\lambda_2^*, y) - E_3 e^{\lambda_3} G(\lambda_3^*, y)\right]. \tag{19}$$

The detailed expression of $G(\lambda, y)$ can be deduced from Duh and Mier-Y-Terán [15] and Henderson *et al.* [14] as

$$G(\lambda, y) = \frac{e^{-\lambda}}{24y}\sum_{n=1}^{5}\frac{V_n(\lambda, y)}{n(T^*)^{n-1}}, \tag{20}$$

where $V_n(\lambda, y)$ are the series expansion coefficients whose explicit expressions can be found in Duh and Mier-Y-Terán [15]. Accordingly, the corresponding contribution to pressure

due to perturbation potential can readily be evaluated from F_t via simple derivative $\frac{\beta P_t}{\rho} = y\left(\frac{\partial \beta F_t}{\partial y}\right)_T$

$$\frac{\beta P_t(y,T)}{\rho} = \beta F_t(y,T) + \frac{12y^2}{T^*}\left[E_1 e^{\lambda_1} G'(\lambda_1^*, y) - E_2 e^{\lambda_2} G'(\lambda_2^*, y) - E_3 e^{\lambda_3} G'(\lambda_3^*, y)\right], \quad (21)$$

where $G'(\lambda^*, y)$ denotes the first derivative of $G(\lambda^*, y)$ with respect to the packing fraction, Y. We carried out quite an involved analytical derivative calculation of $G(\lambda^*, y)$ but the final expressions are quite lengthy to accommodate in the present article. Finally, one can readily derive an analytical expression for the chemical potential, μ, via the standard thermodynamic relations

$$\frac{\beta\mu}{N} = \frac{\beta F}{N} + \frac{\beta P}{\rho}. \quad (22)$$

The remaining parameter that needs to be determined for the present EOS is the effective HS diameter, σ. It is worth noting that the definition of σ is necessarily tied to the use of perturbation theory, and it can be interpreted more generally as the important link between the reference system and the effect of the attractive forces in the fluid modified by a realistic pair interaction [28,29]. In fact there exists several criteria for the choice of σ. Here, we consider two different approaches, for comparison. First, the variational theory of classical fluid [2,26], in which the Helmholtz free energy, F, of the system is an upper bound of the sum of the free energy of reference system (normally, the HS fluid) plus the contribution from attractive potential. Namely,

$$F(\rho, T) \leq F_{HS}(y, T) + F_t(y, T). \quad (23)$$

For clarity, Equation (23) requires the minimisation of the right-hand side with respect to σ, at fixed density and temperature, i.e. $\frac{\partial F(y,T)}{\partial \sigma}|_{\rho,T} = 0$. This optimal approximation for the free energy has been used successfully as part of the pseudopotential theory of liquid metals and is often called the Gibbs–Bogoliubov (GB) variational method [2,26] and was also successfully applied to classical non-metallic fluids [10,29]. The second approach is due to the Barker–Henderson (BH) perturbation theory, in which σ (T) is calculated via simple numerical integration

$$\sigma_{BH}(T) = \sigma_0 \int_0^1 \left[1 - e^{-\beta V_{3YK}(x)}\right] \mathrm{d}x. \quad (24)$$

Here, $x = r/\sigma_0$. It is worth mentioning that the well-known Weeks–Chandler–Andersen (WCA) perturbation scheme [24] may provide relatively more accurate effective HS diameters than both GB and BH prescriptions. The superiority of the WCA method has been demonstrated, in particular for the $V_{GR}(r)$ model potential by Costa *et al.* [30] and Ben-Amotz and Stell [31]. The major problem for applying WCA with the present EOS lies in the difficulty of getting a simple analytical expression of $g(r)$ from the available Laplace transform $G(\lambda, y)$. In practice, applying BH or WCA to the Girifalco type potential may not show dramatic effect to the phase diagram due to the extremely short range between the minimum and zero position of the potential, which is clearly illustrated in Table 1: $r_m - \sigma_0 = 0.0483\sigma_0$. On the other hand, the Lennard–Jones (LJ) potential possesses a much wider range: $r_m - \sigma_0 = 0.1225\sigma_0$. This may explain the importance of WCA for LJ fluids. Moreover, the GB method has the advantage, as it guarantees the thermodynamic

stability of the system via the minimisation of the free energy at each thermodynamic state of T and ρ with respect to the entropy parameter, σ.

4. Thermodynamic properties of C_{60} fluid

In order to locate the L–V coexistence region in the phase diagram, one has to observe the van der Waals loops in the $P-\rho$ or $\mu-\rho$ isotherms. A typical plot of $\mu(\rho, T)$ isotherms is presented in Figure 3. It shows pronounced van der Waals loops for isotherms, $T < T_c$, while the critical isotherm shows a relatively flat inflection point and so extreme points for all isotherms $T > T_c$. Next, we turn to the calculation of the L–V binodal line; first of all, we target a particular $\mu-\rho$ isotherm that exhibits van der Waals loop and solves the non-linear equation,

$$\mu(\rho) - \overline{\mu} = 0, \tag{25}$$

for any arbitrary chemical potential $\overline{\mu}$. The expected three routes are labelled ρ_v for the vapour density, ρ_L for the liquid density and ρ_m for the interfacial state. The second step is to apply the Maxwell equal-area construction rule [32] for the phase equilibrium

$$\int_{\rho_V}^{\rho_m} (\mu(\rho) - \overline{\mu}) \mathrm{d}\rho = -\int_{\rho_m}^{\rho_L} (\mu(\rho) - \overline{\mu}) \mathrm{d}\rho. \tag{26}$$

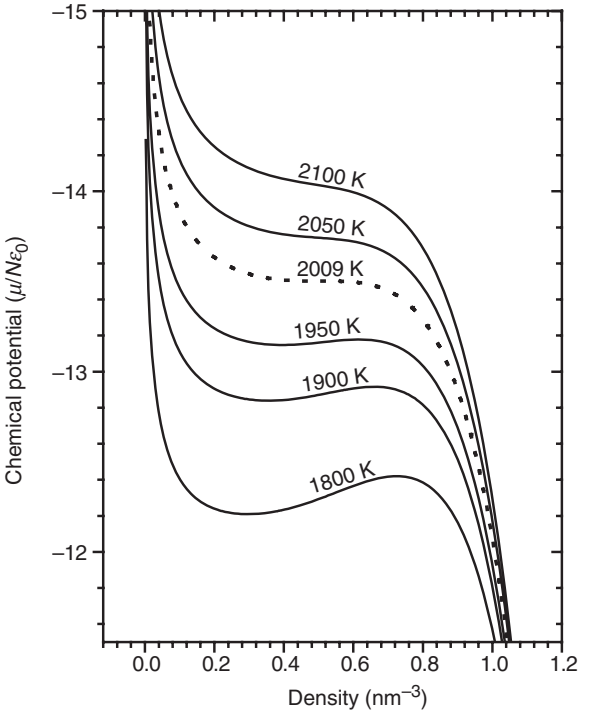

Figure 3. The chemical potential isotherms *versus* number density of C_{60}. The dotted curve refers to the critical isotherm.

Equation (26) only holds for a unique set $(\overline{\mu}, \rho_v, \rho_L)$, which indicates the L–V coexistence densities and chemical potential, such that $\mu(\rho_V) = \mu(\rho_m) = \mu(\rho_L) = \overline{\mu}$. Thirdly, by considering several $\mu - \rho$ isotherms and applying the Maxwell equal-area rule one can generate the whole binodal curve for the fluid of interest. We carried out calculations of two different binodal curves, one using the GB variational method, Equation (23), and the other using the BH formula, Equation (24), for effective HS diameters. A typical L–V coexistence curve for C_{60} is plotted in Figure 4, together with the results of Monte Carlo simulations based on an NVT ensemble [22]. It is clear that the binodal curve based on GB prescription better fits the computer simulations results than that based on the BH method. In general, the BH method is good only at higher temperatures. The NVT-Monte Carlo simulation technique is considered the most accurate method for the LVE calculations as it consistently takes care of the absolute free energy of the fluid phase [22]. Moreover, this energy route-based computer simulation is computationally more demanding as it yields numerically more stable results against size effect errors. The comparison in Figure 4 is reasonable at the whole temperature range except in the near vicinity of the critical point. Figure 5 shows the *P–T* representation of the phase diagram. It appears that the coexisting pressure calculated from the present model agrees well with the NVT-Monte Carlo simulation results at intermediate temperatures. Figure 5 clearly illustrates that the BH prescription to the effective HS diameters largely overestimates the

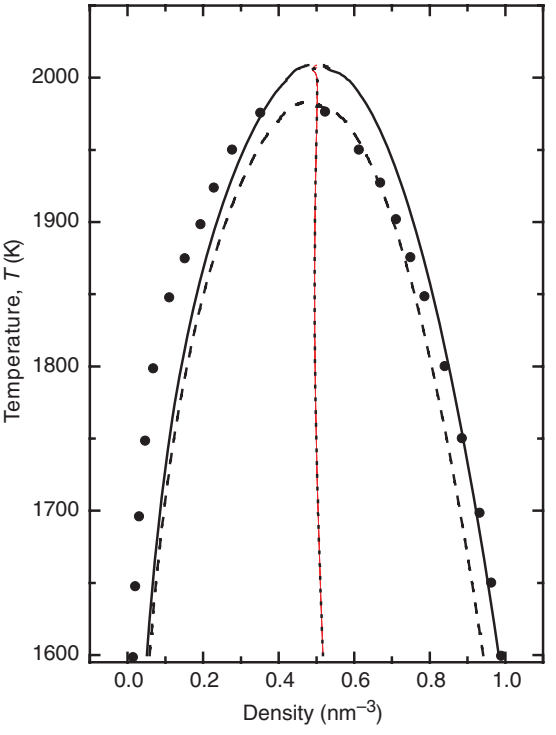

Figure 4. Liquid–vapour coexistence curve for C_{60} using HC3YK potential (solid line for σ_{GB} Equation (23), and dashed line for σ_{BH} Equation (24)) compared with the NVT-Monte Carlo computer simulation result [22] (solid circles). The dotted line shows the rectilinear diameters.

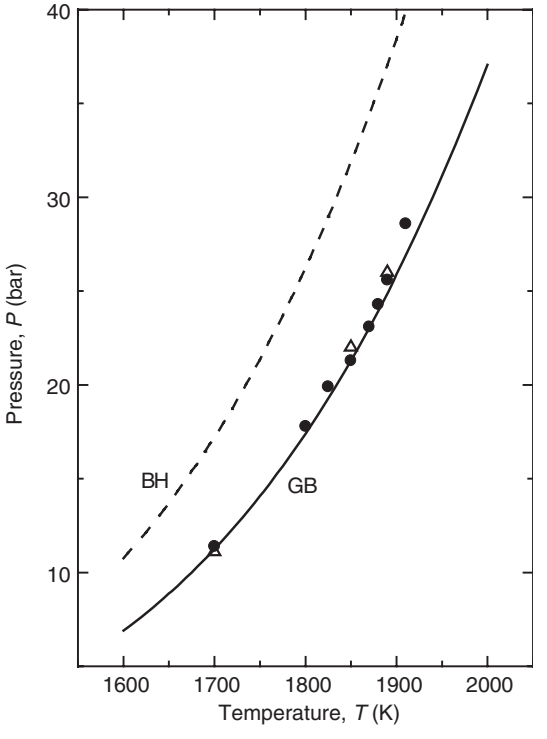

Figure 5. The pressure at LVE for C_{60} using HC3YK potential (solid line for σ_{GB} Equation (23), and dashed line for σ_{BH} Equation (24)) compared with the NVT-Monte Carlo computer simulation result [22] ($N = 600$, solid circles; $N = 1500$, open triangles).

pressure at the whole temperature range. The LVE critical parameters are calculated using a standard extrapolation method [10] and are presented in Table 2. The present EOS estimated critical parameters are compared with the NVT-Monte Carlo computer simulation and other theoretical results [33,3]. In general, the first order perturbation theory overestimates the critical parameters by 15%. Our estimate of the critical parameters T_c and ρ_c compare relatively well with the NVT-Monte Carlo simulation results; their comparison is better than with the HRT and hybrid mean spherical approximation theoretical results. But our critical pressure P_c is largely overestimated. However, P_c of C_{60} is in the same order of magnitude with the critical pressure of Ar, Kr and Xe and also with diatomic liquids N_2, O_2 and CO; also it is in relatively good agreement with polyatomic molecular fluids CO_2, CH_4 and C_6H_6. The most important critical parameter is the compressibility ratio, $Z_c = \frac{P_c}{\rho_c k_B T_c}$, as it exhibits universality for each group of fluids. Guggenheim [34], Chapman and March [35,36] and March [37] have extracted information on the constancy of Z_c at 0.29 for rare gas elements, while for alkali metals, Z_c does not exhibit a universal fixed value, $0.06 \leq Z_c \leq 0.22$. Table 2 provides more information on Z_c for diatomic and polyatomic liquids with covalent bonds. From Table 2, some conclusions may be drawn: (a) the coulomb interaction is crucial in understanding the lower value of Z_c in case of alkali metals; (b) the bonding effect in diatomic fluids does not alter the universal value ($Z_c \approx 0.29$), while in polyatomic liquids,

Table 2. Critical parameters of C_{60} compared with the most recent computer simulations (NVT-Monte Carlo, NPT-Monte Carlo and GEMC) and with theoretical results (HRT and HMSA) based on integral equation methods. Also compared with experimental data for some metals, non-metals and organic elements.

	Reference	Molecular weight ($g\,mol^{-1}$)	T_c (K)	ρ_c (g/cm^3)	P_c (bars)	Z_c
C_{60}	Present work	720.669	2008.8	0.5985	53.05	0.379
	NVT-Monte Carlo [22]		1980	0.5325	36.6	0.301
	NVT & NPT-Monte Carlo [23]		1940	0.5025	27.0	0.240
	GEMC [42]		1941	0.5025	29	0.27
	HRT [33]		2138	0.5983	46.5	0.315
	HMSA [3]		2050	0.6701		
Li	[37,43]	6.939	1615	0.3086	274.7	0.046
Na	[38]	22.989	2600	0.21	280	0.142
K	[38]	39.10	2200	0.19	150	0.169
Rb	[38]	85.467	2100	0.35	160	0.217
Cs	[38]	132.9055	2030	0.44	110	0.203
Hg	[38]	200.5	1760	5.7	1520	0.365
He	[44,45]	4.0036	5.188	0.0655	2.29	0.325
Ne	[34]	20.18	44.8	0.4840	27.25	0.305
Ar	[34,46]	39.94	150.7	0.5308	48.62	0.292
Kr	[34,46]	83.7	209.4	0.9083	54.8	0.290
Xe	[34,47]	131.3	289.75	1.116	58.96	0.288
H_2	[48]	2.016	20.268	0.0899	1.013	0.014
N_2	[34]	28.02	126.0	0.311	33.94	0.292
O_2	[34]	32.0	154.3	0.430	50.346	0.292
CO	[34]	28.019	133.0	0.301	34.95	0.294
CO_2	[44]	44.009	304.0	0.468	73.75	0.274
CH_4	[34]	16.03	190.3	0.162	46.29	0.290
H_2O	[49]	18.0152	647	0.3252	215.2	0.227
NH_3	[49]	17.0304	406	0.2365	110.56	0.242
n-Pentane C_5H_{12}	[44]	72.15	470.0	0.233	33.73	0.267
neoPentane C_5H_{12}	[44]	72.15	434.0	0.2385	32.02	0.268
Benzene C_6H_6	[44]	78.11	563.0	0.2582	49.23	0.318

the bonding effect is lowering this value; and (c) the quantum effect in Ne, He and H_2 is responsible for increasing Z_c up to 0.33 with ascending order as the quantum effect increases i.e. $Z_c^{Ne} < Z_c^{He} < Z_c^{H_2}$. However, there is no obvious explanation in the literature on how Z_c depends on the number of bonds or on the quantum effect. Owing to the fact that C_{60} molecules possess extremely short ranged and strongly attractive intermolecular potential, we expect large differences in its critical parameters comparable with those of noble gas metals, alkali metals or transition metals, which possess soft cores and quite a long range coulomb attractive tail. However, the comparison in Table 2 with other real fluids is not intended to test the accuracy of the present EOS, but to show how C_{60} fluid can be categorised among other systems.

The comparisons in Figures 2, 4 and 5 indicate reasonable accuracy of the present EOS and allow an accurate investigation for the coexistence of thermodynamic properties. Thermodynamic functions are then derived in the usual way by taking the appropriate

derivatives of Equations (11) and (12). One can readily derive analytical expressions for the isothermal compressibility, κ_T, adiabatic compressibility, κ_S, the thermal pressure coefficient, α_V, the coefficient of thermal expansion at constant pressure (expansibility), α_P, isochoric and isobaric heat capacities, C_V, C_P, respectively, and the total entropy, S, via the following thermodynamic relations [38,39]:

$$\kappa_T = \frac{1}{\rho}\left(\frac{\partial \rho}{\partial P}\right)_T, \tag{27a}$$

$$\kappa_S = \frac{1}{\rho}\left(\frac{\partial \rho}{\partial P}\right)_S = \frac{K_T}{\gamma}, \tag{27b}$$

$$\alpha_V = \left(\frac{\partial P}{\partial T}\right)_\rho, \tag{28a}$$

$$\alpha_P = -\frac{1}{\rho}\left(\frac{\partial \rho}{\partial T}\right)_P = \kappa_T \alpha_V, \tag{28b}$$

$$C_V = -T^2\left(\frac{\partial^2 F}{\partial T^2}\right)_\rho, \tag{29a}$$

$$C_P = C_V + \frac{T}{\rho \kappa_T}\alpha_P^2 = C_V + \frac{T}{\rho}\kappa_T \alpha_V^2, \tag{29b}$$

$$\frac{S}{Nk_B} = -\left(\frac{\partial F}{\partial T}\right)_\rho, \tag{30}$$

where the heat capacity ratio

$$\gamma = \frac{C_P}{C_V}. \tag{31}$$

All thermodynamic functions are calculated from the present EOS along the LVE. The compressibility, one of the important thermodynamic properties, is given by the second derivative of the partition function, which determines the stability of the fluid and can be used to calculate the zero frequency limit of the speed of sound, $v_s = \sqrt{\frac{\gamma}{m\rho\kappa_T}}$. In particular, the isothermal compressibility can be calculated from the present EOS via Equation (27a), and can also be calculated from the cyclic relation $\kappa_T = -\alpha_P/(\rho^2(\partial S/\partial \rho)_T)$, where S is the total entropy of the system, Equation (30). This indicates the sensitivity of κ_T to both pressure and structure changes. Figure 6(a) shows the behaviour of κ_T in vapour and liquid phases. κ_T is nearly zero for liquid phases far from the critical point up to ≈50 K below T_c, then diverges sharply as $T \to T_c$. Remarkably, κ_T for the vapour phase shows ideal gas-like behaviour, $\kappa_T = 1/\rho k_B T$ at low temperatures and reverses to a liquid-like behaviour at $T \geq 1902$ K. The adiabatic compressibility, κ_S, is plotted in Figure 6(b). It is almost zero for the liquid phase, with a slight increase as $T \to T_c$, which indicates that the packing of molecules in the liquid phase is almost independent of temperature. On the contrary, the sharp decrease of the vapour phase κ_S indicates the continuous packing of vapour

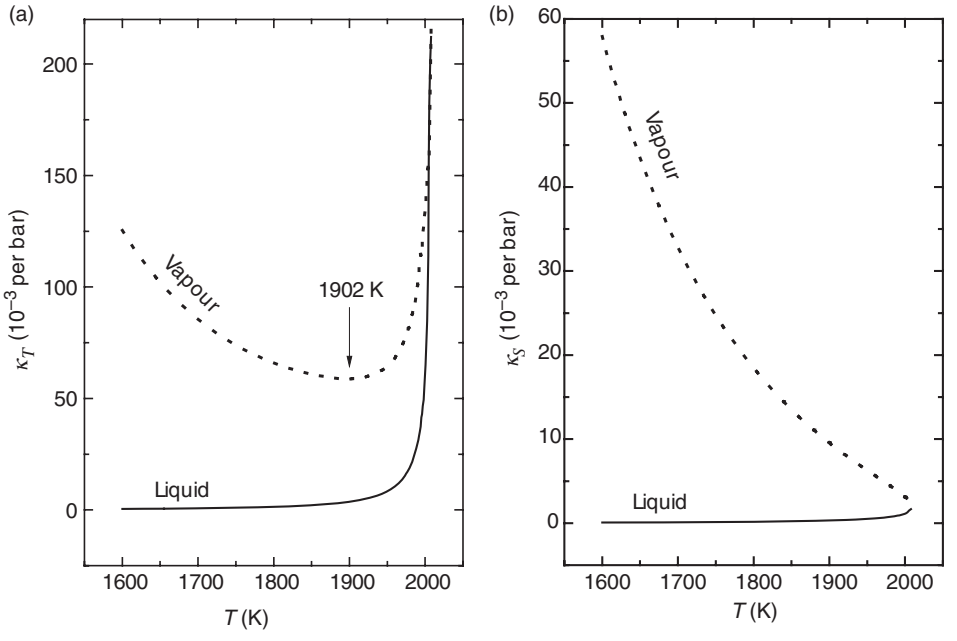

Figure 6. (a) Temperature dependence of isothermal compressibility, κ_T, Equation (27a), of C_{60} for both liquid and vapour phases at equilibrium, (b) temperature dependence of the adiabatic compressibility, κ_S, Equation (27b), of C_{60} for both liquid and vapour phases at equilibrium.

molecules by increasing temperature and pressure. At critical point, $K_S^{Vapour} = K_S^{Liquid}$, which means that both phases are equally packed and hence they are indistinguishable.

On the other hand, the pure chemicals can be characterised by their thermomechanical properties, such as isochoric pressure coefficient, α_V, and isobaric expansibility, α_P, which can be easily calculated from the EOS by taking the respective temperature derivatives, Equations (28a) and (28b), respectively. The ideal gas limit $\alpha_P^{id} = \frac{1}{T}$ and $\alpha_V^{id} = \frac{P}{T}$. Figure 7(a) and (b) shows α_P and α_V, respectively, along the L–V coexistence curve. Figure 7(a) shows that both vapour and liquid typically expand at the same rate, with maximum expansibility at the near vicinity of the critical point, while Figure 7(b) illustrates the fact that the vapour phase responds more dramatically with pressure variations for any small temperature fluctuations than the liquid phase. In other words, the liquid phase is more mechanically stable than the vapour phase under thermal expansion. Quite recently, March and Angilella [40] have explored the usefulness of α_V and α_P together with their interrelation to the isothermal compressibility κ_T to obtain a new EOS for H_2O and NH_3 near the critical point, which is very important in explaining the validity of the inequality between the shear viscosity and entropy density.

The configurational heat capacity, C_V, is a purely thermodynamic property used particularly to measure the performance of a theory, and can therefore measure the influence of higher order terms in the perturbation expansion. Moreover, the characteristic function C_V provides an important measure of the influence of the structure

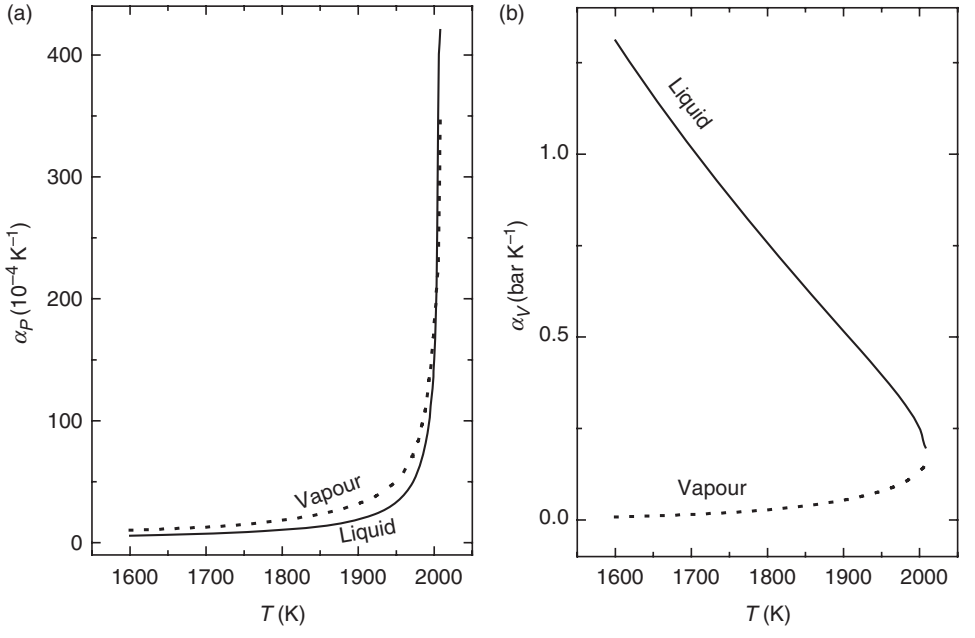

Figure 7. (a) The coefficient of thermal expansion, α_P, Equation (28b) of C_{60} versus temperature along the LVE curve, (b) thermal pressure coefficient, α_V, Equation (28a) of C_{60} versus temperature along the LVE curve.

and forces on the state of a fluid. Figure 8(a) shows C_V *versus* temperature. It is clear that the vapour phase C_V is much higher than that of the liquid phase, which can be interpreted due to the influence of the higher kinetic energy of the vapour molecules. However, as $T \to T_c$, both phases possess equal heat capacities. The vapour phase C_V shows a maximum value at $T \simeq 1955\,\mathrm{K}$ and reverses behaviour by increasing temperature. The decrease in C_V can be attributed to the clustering process that may take place due to the increase of pressure while the vapour approaches its critical state. According to the classical theory of critical phenomena, the constant pressure heat capacity C_P strongly diverges as $T \to T_c$. Moreover, $C_P \to \propto$ provides a rather stringent critical condition for a particular theoretical approach. Figure 8(b) shows strong divergence of C_P at the near vicinity of the critical point. However C_P of the liquid phase diverges more strongly than that of the vapour phase. The heat capacity ratio, $\gamma = C_P/C_V$, was explored by several authors [36–39,41] without decisive conclusion. For most simple liquids, the γ parameter does not vary widely near the melting point and diverges sharply, as C_P, near the critical point. In addition, γ also correlates with the ratio of isothermal to adiabatic compressibilities, as in Equation (27b). A typical plot of γ versus temperature is given in Figure 8(c), which shows a relatively fixed value of γ for a wide range of temperature and a dramatic increase at the near vicinity of the critical point. Figure 9 shows the entropy of both phases calculated via Equation (30). It shows a high degree of symmetry of liquid and vapour structure when they expand to a less ordered state towards the critical state; eventually, an equal entropy is achieved, indicating no structural distinction as $T \to T_c$.

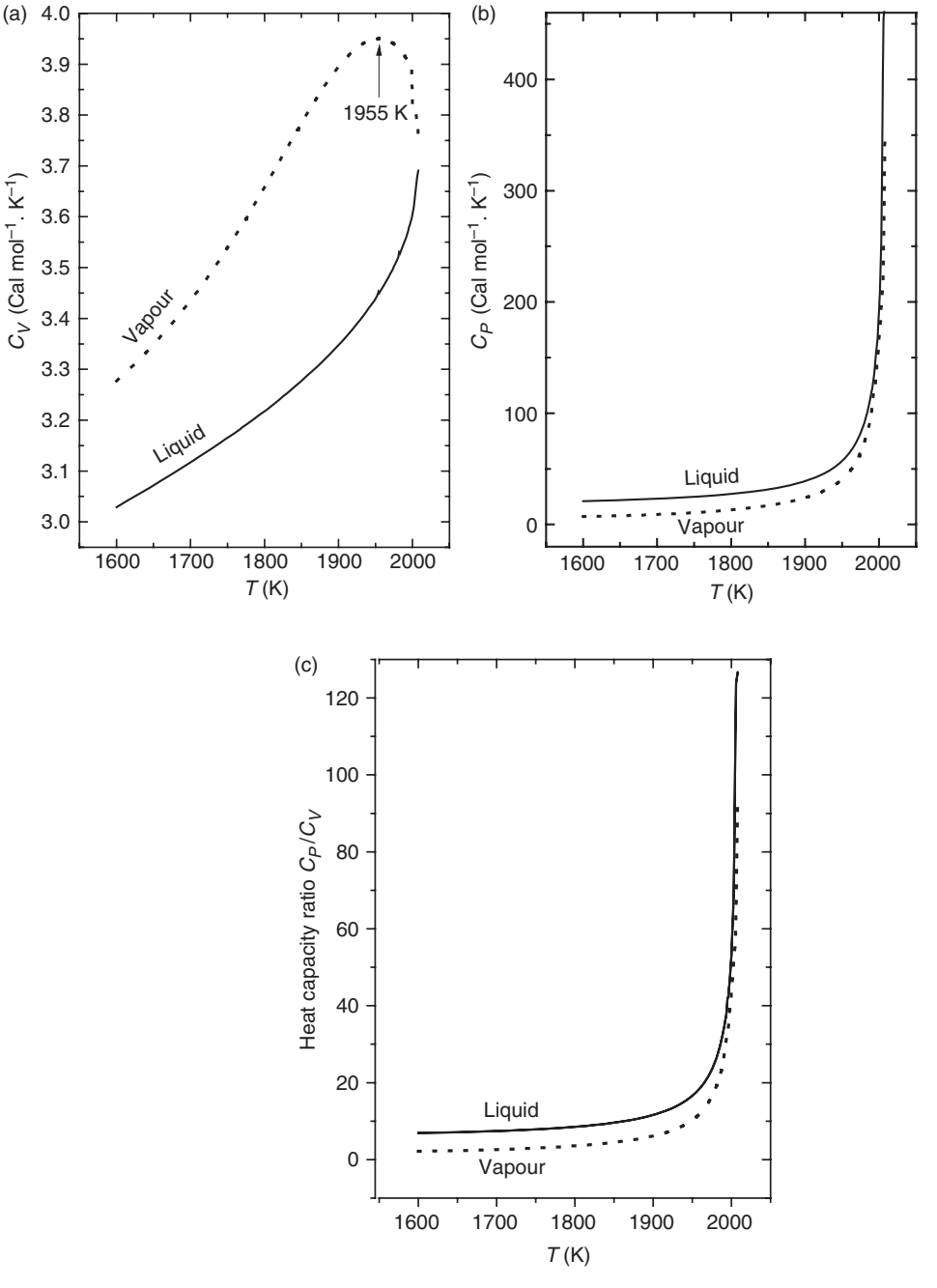

Figure 8. (a) Constant volume heat capacity, C_V, Equation (29a), of C_{60} along the LVE curve; (b) isobaric volume heat capacity, C_P, Equation (29b), of C_{60} along the LVE curve; (c) the heat capacity ratio $\gamma = C_P/C_V$ plotted against equilibrium temperature for both liquid and vapour phases of C_{60}.

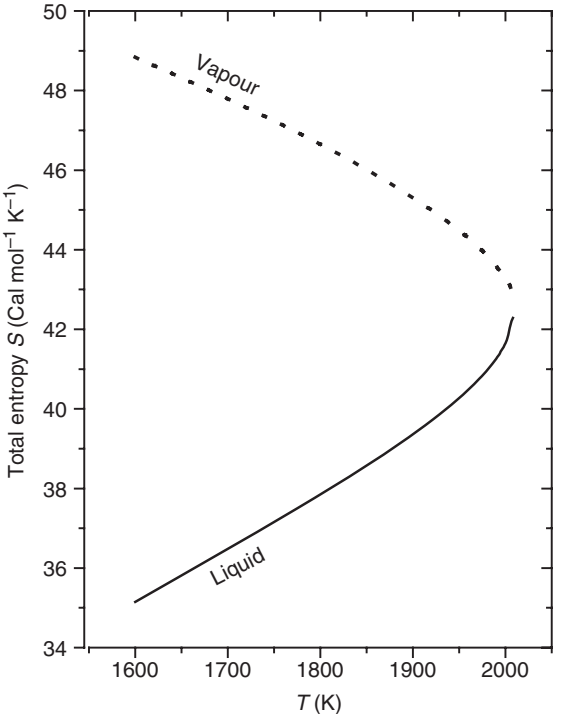

Figure 9. The temperature dependence of the total entropy, Equation (30), along the LVE curve.

5. Conclusion

A new EOS for C_{60} is presented and employed to locate the liquid–vapour binodal curve, and also used to calculate most thermodynamic properties of the equilibrium phases. The new EOS is based on the first-order perturbation theory of fluids, for which the main ingredients are (a) the HS reference system formalism taken from a recent development of the scaling theory, (b) the HC3YK potential which is accurately designed to mimic the original C_{60} interaction potential, (c) the analytical expressions of the Laplace transform $G(\lambda, y)$ of the radial distribution function, and (d) the Gibbs–Bogoliubov variational approach for the effective HS diameters. The quality of the HC3YK potential as well as the present EOS is assessed by consulting the computer simulation results of (a) the second virial coefficient $B_2(T)$, (b) the $\rho - T$ results of the binodal curve, and (c) the L–V equilibrium pressure–temperature relation. These comparisons are satisfactory and enabled us to proceed in investigating the behaviour of the most important thermodynamic functions of the two phases at equilibrium state. All thermodynamic functions of interest show the expected qualitative behaviour of the liquid phase typically, as in the case of expanded non-conducting fluids, while for the gas phase behaviour changes from ideal gas to cluster formation tendency at $\approx$50 K below the critical point; however, this problem is still wide open for further investigation. The critical parameters of C_{60} are compared with those of different classes of liquids.

Acknowledgements

The authors are grateful to the Sultan Qaboos University for the Research Project IG/Sci/Phys/07/04. M. Bahaa Khedr would like to thank SQU for hospitality and substantial financial support for completing this work.

References

[1] O. Zhou and D.E. Cox, J. Phys. Chem. Solids **53**, 1373 (1992).
[2] N.W. Ashcroft, Europhys. Lett. **16**, 355 (1991).
[3] A. Cheng, M.L. Klein, and C. Caccamo, Phys. Rev. Lett. **71**, 1200 (1993).
[4] C. Rey, L.J. Gallego, and J.A. Alonso, Phys. Rev. **B49**, 8491 (1994).
[5] M. Hasegawa and K. Ohno, J. Phys. Cond. Matter **9**, 3361 (1997).
[6] M.H.J. Hagen, H.J. Heijer, G.C.A.M. Mooij, and H.N.W. Lekkerkerker, Nature **365**, 425 (1993).
[7] L. Mederos and G. Navascués, Phys. Rev. **B50**, 1301 (1994).
[8] M. Hasegawa and K. Ohno, Phys. Rev. **E54**, 3928 (1996).
[9] C. Caccamo, Phys. Rev. **E51**, 3387 (1995).
[10] M. Bahaa Khedr, M.S. Al-Busaidy, and S.M. Osman, J. Phys.: Condens. Matter **17**, 4411 (2005).
[11] A. Parola and L. Reatto, Adv. Phys. **44**, 211 (1995).
[12] D. Pini, G. Stell, and N.B. Wilding, Mol. Phys. **95**, 483 (1998).
[13] E. Scholl-Paschinger and G. Kahl, Europhys. Lett. **63**, 538 (2003).
[14] D. Henderson, L. Blum, and J.P. Noworyta, J. Chem. Phys. **102**, 4973 (1995).
[15] D.-M. Duh and L. Mier- Y-Terán, Mol. Phys. **90**, 373 (1997).
[16] M.C. Abramo, C. Caccamo, D. Costa, and G. Pellicane, Europhys. Lett. **54**, 468 (2001).
[17] L.A. Girifalco, J. Phys. Chem. **96**, 858 (1992).
[18] H. Guerin, J. Phys. Cond. Matter **10**, L527 (1998).
[19] J.M. Pacheco and J.P. Prates-Ramalho, Phys. Rev. Lett. **79**, 3873 (1997).
[20] M.C. Abramo, C. Caccamo, D. Costa, G. Pellicane, and R. Ruberto, Phys. Rev. **E69**, 31112 (2004).
[21] J.Q. Broughton, J.V. Lill, and J.K. Johnson, Phys. Rev. **B55**, 2808 (1997).
[22] M. Hasegawa and K. Ohno, J. Chem. Phys. **111**, 5955 (1999).
[23] D. Costa, G. Pallicane, M.C. Abramo, and C. Caccamo, J. Chem. Phys. **118**, 304 (2003).
[24] J.P. Hansen and I.R. McDonald, *Theory of Simple Liquids* (Academic Press, London, 1976).
[25] N.F. Carnahan and K.E. Starling, J. Chem. Phys. **51**, 635 (1969).
[26] W.H. Young, Rep. Prog. Phys. **55**, 1769 (1992).
[27] M. Baus and J.L. Colot, Phys. Rev. **A36**, 3912 (1997).
[28] S. Bastea, Phys. Rev. **E68**, 031204 (2003).
[29] I. Ali, S.M. Osman, M. Al-Busaidi, and R.N. Singh, Int. J. Mod. Phys. **B13**, 3261 (1999).
[30] D. Costa, G. Pellicane, and C. Caccamo, Phys. Rev. **E68**, 021104 (2003).
[31] D. Ben-Amotz and G. Stell, J. Chem. Phys. **119**, 10777 (2003).
[32] J.S. Rowlinson and B. Widom, *Molecular Theory of Capillarity* (Clarendon Press, Oxford, 1982).
[33] M. Tau, A. Parola, D. Pini, and L. Reatto, Phys. Rev. **E52**, 2644 (1995).
[34] E.A. Guggenhein, J. Chem. Phys. **13**, 253 (1945).
[35] R.G. Chapman and N.H. March, Phys. Chem. Liq. **16**, 77 (1986).
[36] R.G. Chapman and N.H. March, Phys. Chem. Liq. **17**, 165 (1987).
[37] N.H. March, J. Non-Cryst. Solids **250-252**, 1 (1999).
[38] M. Shimoji, *Liquid Metals: An Introduction to the Physics and of Metals in the Liquid State* (Academic Press, London, 1977).

[39] M.W. Zemansky and R.H. Dittman, *Heat and Thermodynamics: An Intermediate Textbook*, 6th ed. (McGraw-Hill, London, 1981).
[40] N.H. March and G.G.N. Angilella, Phys. Chem. Liq. **47**, 344 (2009).
[41] L. Carrarese, M. Celli, and F. Barocchi, Phys. Chem. Liq. **25**, 91 (1993).
[42] C. Caccamo, D. Costa, and A. Fucile, J. Chem. Phys. **106**, 255 (1997).
[43] R. Hultgren, P.D. Desai, D.T. Hawkins, M. Gleiser, K.K. Kelley, and D.D. Wagman, *Selected Values of the Thermodynamic Properties of the Elements* (American Society for Metals).
[44] I.O. Hirschfelder, C.F. Curtiss, and R.B. Bird, *Molecular Theory of Gases and Liquids* (Wiley, New York, 1954).
[45] S.S. Leung, Phys. Rev. A **8**, 2670 (1973).
[46] W.B. Street, Physica **71**, 51 (1974).
[47] U. Nager and D. Balzarini, Phys. Rev. B **42**, 6651 (1990).
[48] Q. Wang, J.K. Johnson, and J.Q. Broughton, Mol. Phys. **89**, 1105 (1996).
[49] N.H. March and M.P. Tosi, *Introduction to Liquid State Physics* (World Scientific, Singapore, 2002).